ARTICLE NO. 79-0758R

J80-213

Elastic-Plastic Analysis of Fatigue Crack Closure in Modes I and II

30003
80004
80005

M. Nakagaki* and S.N. Atluri†
Center for the Advancement of Computational Mechanics, Georgia Institute of Technology, Atlanta, Ga.

An efficient elastic-plastic finite element procedure to analyze crack closure and its effects on fatigue crack growth under general spectrum loading is presented. A hybrid-displacement finite element procedure is used to treat properly the stress and strain singularities near the crack tip; and crack growth under cyclic loading is simulated by the translation of certain "core" elements, near the crack tip, in which proper stress and strain singularities were embedded. Both pure mode I and mode II types of cyclic loading are considered. In the mode I case, four types of cyclic loadings, i.e., constant amplitude block loading, high-to-low block loading, low-to-high block, and a single overload in an otherwise constant amplitude block loading, are considered. The stress level at which crack growth occurs is selected on the basis of experimental results reported in literature. In the case of mode II, only a constant amplitude block loading is considered. Detailed results are presented for crack closure and opening stresses, crack surface deformation profiles, etc., in each case. Certain observations, based on the present numerical results, concerning various factors that cause crack-growth acceleration or retardation under general spectrum loading are presented and discussed.

Introduction

As discussed recently by Schijve,[1] the mechanism of crack closure, as first observed experimentally by Elber,[2] is generally considered to be a predominant mechanism that contributes to "interaction effects," which cause crack-growth retardation or acceleration under variable-amplitude fatigue loading. It is also generally understood[1] that the crack-closure phenomenon is caused by residual plastic deformations remaining in the wake of the advancing crack tip, as initially postulated by Elber. Analytical models that lend theoretical support to the existence of crack-closure phenomenon in fatigue crack growth, and provide some rationality for the adoption of an effective stress-intensity range based on closure effects for the correlation of fatigue crack-growth rates, have also been proposed by Budiansky and Hutchinson.[3] As for a more general analysis of extending cracks under general block cyclic loading to obtain crack-closure stresses, crack-opening stresses, details of crack-surface deformations, and residual stresses in the crack-tip region, etc., elastic-plastic finite element analysis was first performed by Newman and colleagues.[4,5] Apart from these analyses, the authors are aware of similar attempts only by Ohji et al.[6-7] The studies in Refs. 4-7 considered the mode I case only. Also, since the crack growth was simulated in Refs. 4-7 by shifting a finite element node (the current crack tip) to an immediately adjacent node, and since constant strain, triangle-type finite elements were used to model the cracked structure, a very fine finite element mesh (with the smallest element often being of the order of 10^{-3} times the crack length) is necessary in their modeling procedures. Thus, the finite element computations of the type given in Refs. 4-7 can be very expensive, especially when cyclic loading of arbitrary spectrum is considered.

Presented herein is an alternate cost-effective and accurate elastic-plastic finite element procedure to analyze fatigue crack closure and its effects under general spectrum loading. In this procedure, the well-known Hutchinson-Rice-Rosengren[8,9] type strain and stress singularities for strain-hardening materials are embedded in specially developed elements near the crack tip. This eliminates the need for a very fine mesh near the tip. For instance, the crack-tip elements in the present procedure are of the order of 10^{-1} of the crack length, as compared to constant strain triangles of the order of 10^{-3}-10^{-4} times the crack-length generally used in the procedures of Refs. 4-7. A hybrid-displacement finite element mthod[10-11] is used in developing these special elements. Also, in the present procedure, crack growth is simulated by the translation of a core of the aforementioned special elements by an arbitrary amount in the desired direction. Since the aforementioned special elements near the crack tip are of circular-sector shape, centered at the crack tip, crack growth in an arbitrary direction from the initial-crack axis, under general mixed mode cyclic loading, can be modeled. The presently considered cases of crack-geometries and far-field applied loading result in "small-scale" yielding conditions near the crack tip. In these cases, a static-condensation procedure, which results in a considerable economy of computer time, is employed.

In the present paper, both mode I and II cases of cyclic loadings of the type previously described are considered. Detailed results are presented for crack-opening and -closure stresses, crack-surface deformation profiles, and effective stress-intensity factor ranges for fatigue crack growth, in each case of block loading. Also presented are detailed discussions, based on the obtained numerical results, concerning various factors that cause crack growth acceleration or retardation and delay effects under different types of cyclic loading.

Mathematical Details of Analysis Procedure

An incremental updated Lagrangian finite element formulation for finite-deformation elasto-plasticity is used herein. The flow theory of plasticity that is used is characterized by the well known Huber-Mises-Hencky initial yield criterion and a Prager-Ziegler type kinematic hardening rule. Circular-sector-shaped singularity elements (in which a displacement field that corresponds to the forementioned Hutchinson-Rice-Rosengren singularities in strains and stresses for strain-hardening elasto-plastic materials are

Presented as Paper 79-0758 at the AIAA/ASME/ASCE/AHS 20th Structures, Structural Dynamics & Materials Conference, St. Louis, Mo., April 4-6, 1979; submitted May 11, 1979; revision received Feb. 21, 1980. Copyright © American Institute of Aeronautics and Astronautics, Inc., 1979. All rights reserved.

Index categories: Structural Durability; Structural Design; Analytical and Numerical Methods.

*School of Civil Engineering; currently with Naval Research Laboratory, Washington, D.C.

†Regents' Professor of Mechanics, School of Civil Engineering. Member AIAA.

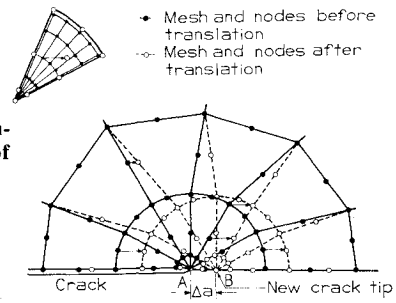

Fig. 1 Schematic representation of translation of singular elements.

embedded) are used near the crack tip, as shown in Fig. 1. These singular elements are surrounded by "regular" eight-noded isoparametric quadrilateral elements, also shown in Fig. 1. Compatibility of displacements and reciprocity of tractions between these "singular" and "regular" elements are enforced through a Lagrangian multiplier technique (thus leading to a "hybrid" element formulation), as shown below.

Let y_i^N be the current (say, in a state C_N) Cartesian spatial coordinates of a particle, to be used as a reference system for the current increment, i.e., from C_N to C_{N+1}. Let τ_{ij}^N be the true (Cauchy) stress in C_N. and let S_{ij} $(\equiv S_{ij(N)}^{N+1} - \tau_{ij}^N)$ be the rate of second Piola-Kirchhoff (P-K) stress referred to C_N. It is noted that $S_{ij(N)}^{N+1}$ is the second P-K stress in state C_{N+1} as referred to C_N. Let $\dot{u}_i$ represent the rate of deformation from C_N, and let $\dot{u}_{i,j} \equiv \partial \dot{u}_i / \partial y_j^N$. Also, let elements $m = 1,2,...p$ be the sector-shaped singularity elements, and $m = p+1...M$ be the surrounding regular elements. It can be shown that the variational principle governing: 1) the conditions of equilibrium in each element (singular as well as regular), 2) traction boundary conditions for each element, where such exist, and 3) conditions of compatibility of displacements and reciprocity of tractions between singular and regular elements can be stated as the stationary condition of the functional:

$$
\begin{aligned}
F &= F_s(\dot{u}_i; \dot{v}_i; \dot{T}_{Li}) + F_R(\dot{v}_i) \\
&\equiv \sum_{m=1}^{P} \left(\int_{\Omega_m} \left\{ \dot{W}(\dot{u}_i) - \rho^N \underline{\underline{B}}_i \dot{u}_i + (1/2) \tau_{ij}^N \dot{u}_{k,i} \dot{u}_{k,j} \right\} \mathrm{d}\Omega \right. \\
&\quad \left. - \int_{S_{\sigma_m}} \dot{\bar{T}}_i \dot{v}_i \mathrm{d}s - \int_{\partial\Omega_m} \dot{T}_{Li} (\dot{u}_i - \dot{v}_i) \mathrm{d}s \right) \\
&\quad + \sum_{m=P+1}^{M} \left(\int_{\Omega} \left\{ \dot{W}(\dot{v}_i) - \rho^N \dot{B}_i \dot{u}_i + (1/2) \tau_{ij}^N \dot{u}_{k,i} \dot{u}_{k,j} \right\} \mathrm{d}\Omega \right. \\
&\quad \left. - \int_{S_{\sigma_m}} \dot{\bar{T}}_i \dot{v}_i \mathrm{d}s \right)
\end{aligned}
\tag{1}
$$

where F_s is the functional for the group of singular elements and F_R is that for the group of regular elements. Thus, in the singular element one assumes: 1) an arbitrary displacement field $\dot{u}_i$ within the element Ω_m to include the proper strain/stress singularities as well as nonsingular polynomial variations; 2) an independent displacement field v_i at the singular-element boundary $\partial\Omega_m$ and 3) Lagrange multiplier T_{Li} at the boundary to enforce the constraint $\dot{u}_i = \dot{v}_i$ at the boundaries of singular elements. In the regular elements, developed through the usual compatible displacement method, one assumes a single compatible displacement field $\dot{v}_i$. Thus, it is seen that if v_i at the boundary of a singular element is so chosen that it matches with the $\dot{v}_i$ of regular elements at the interfaces of singular and regular elements, total displacement compatibility is enforced throughout the structure.

Also, in Eq. (1), $\dot{W}$ is the rate potential for the rate of second P-K stress $\dot{S}_{ij}$ such that, $\partial \dot{W} / \partial \dot{\epsilon}_{ij} = \dot{S}_{ij}$, where $\dot{\epsilon}_{ij}$ is the updated Lagrangian strain rate, $\dot{\epsilon}_{ij} = 1/2(\dot{u}_{i,j} + \dot{u}_{j,i})$. This rate potential has been consistently derived from a postulated rate potential for the corotational (Jaumann) rate of Kirchhoff stress, using the well-known classical rate theories of (finite deformation) rate-independent elasto-plasticity, as discussed in detail elsewhere.[12,13]

The details of assumed variables $\dot{u}_i, \dot{v}_i$, and $\dot{T}_{Li}$ for the singular elements are omitted here. However, for the present purposes, it is worth noting that each sector-shaped singular element has three nodes along the circumference, and four nodes along each of the radial boundary lines. Along the circumferential boundary, the field $\dot{v}_i$ is assumed in the form

$$\dot{v}_i = a_{1i} + a_{2i}\theta + a_{3i}\theta^2 \tag{2}$$

where θ is the circumferential angle, and $a_{1i}...a_{3i}$ are expressed in terms of the respective displacements at the three nodes along the circumference. It can be seen that the above boundary displacement $\dot{v}_i$ is compatible with that of the surrounding eight-noded isoparametric quadrilaterals. Along the radial boundaries of the singular elements, $\dot{v}_i$ is assumed as

$$\dot{v}_i = b_{1i} + b_{2i}r + b_{3i}r^2 + b_{4i}r^{1/n+1} \tag{3}$$

where r is the radial distance from the crack tip; n is the exponent in the material hardening law (i.e., from the uniaxial stress-strain curve, $\epsilon_p \sim \sigma^n$; ϵ_p is the plastic strain, and σ the stress); and the coefficients $b_{1i}...b_{4i}$ are expressed in terms of the respective nodal displacements at the aforementioned four nodes.

Finally it is noted that the variational principle in Eq. (1) assumes that the current state C_N is exactly equilibrated. In general, such is not the case; hence, equilibrium correction iterations of the Newton-Raphson type have to be performed at the end of each incremental solution. The details of these iterations have already been presented elsewhere.[11,12]

Finite Element Modeling of Crack Growth

The steps in the finite element simulation of crack growth in the present procedure may be described as: 1) geometrical change in the crack surface boundary, 2) translation of the crack-tip singularities to the advanced crack tip, and 3) release of surface tractions on the newly created crack surface.

The change in the crack surface boundary is made by translating the whole set of crack-tip core elements, as shown in Fig. 1, by arbitrary distance Δa in the direction of intended crack extension. Thus the new crack-tip node, which is designated by the center of the sector-shaped core elements, need not be coincident with any previously existing finite element node before extension. Thus, even though the fixed boundary in the uncracked ligament of the structure changes, the constraining condition of the nodes need not be altered. Elements immediately adjacent to the core must be readjusted to fit to the translated core. This process of translating the core mesh also moves the embedded singularity in the elements to the new crack-tip area, leaving no singularities but large deformations and strains in the wake of advanced crack tip. All of the 5×5 Gaussian data points in each of the translated core elements (and also the 5×5 points for the conventional elements) may generally not coincide with those before translation, when plastic history data such as current stresses, plastic strains, plastically dissipated work, yield surface translation, etc., are available. Therefore, the data at points in the new mesh are estimated by linearly interpolating data on four Gaussian points in the old mesh that are nearest to the point under question in the new mesh. The simple but cumbersome mathematical details of this interpolation and smoothing process are omitted here for the sake of brevity. With the fitted plastic data and the new element geometry, element stiffness matrices are recalculated for the core elements as well as for the surrounding rearranged elements, and the global stiffness is appropriately modified. Subsequent equilibrium check iterations using the new stiffness of the structure correct fitting errors, if any, in the plasticity data in the new mesh. At the same time, the tractions over the

distance AB (Δa as shown in Fig. 1) are incrementally removed, with equilibrium check iterations being used at each step to create a new traction-free crack surface of length Δa. The finite element simulation of crack extension by the desired amount, Δa, is now completed.

Analysis of Fracture Crack Growth Under Mode I Cyclic Loading: Description of the Problem

Throughout the series of the present elastic-plastic finite element analyses of fatigue crack growth under mode I type cyclic loading, a thin rectangular plate with a central crack and under uniform tensile stresses, in a direction normal to the crack-axis at the edges of the plate, is considered (Fig. 2). The dimensions of the plate are: half width $w = 230$ mm and half-crack length $a_0 = 27.3$ mm. The material is a 2024-T3 aluminum alloy whose mechanical properties are characterized by a yield stress $\sigma_{ys} = 350$ MN/m^2, and Young's modulus $E = 70{,}000$ MN/m^2. The material is assumed to be elastic-perfectly-plastic. It is noted that the above problem definition is identical to that used by Newman.[5] The plate is assumed to be in a state of plane stress.‡

Because of the symmetries of geometry, applied loading, and material homogeneity, only a quarter of the cracked plate is analyzed. Figure 2 shows the finite element breakdown that is used. A total of 6 sector-shaped singularity elements near the crack tip and 43 conventional quadratic isoparametric elements are employed. Some of these isoparametric elements are 6-noded triangles, while the majority are 8-noded quadrilaterals (see Fig. 2). It is seen that the number of nodes in the finite element mesh for the quarter-plate is 171, with a total of 311 degrees of freedom.

The radius of the sector-shaped singularity elements is chosen as $\rho = 2.8$ mm; i.e., $\rho/a_0 = .103$. While the crack-extension per cycle of loading, Δa, can be arbitrary (i.e., not related to the finite element mesh size) in the present analysis procedure, it is chosen to be $\Delta a = 0.14$ mm in the present series of computations.

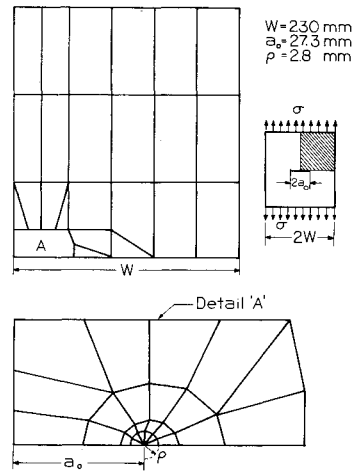

Fig. 2 Finite element model of a center-cracked specimen under uniaxial cyclic loading (Singular Elements Shown Within Detail A).

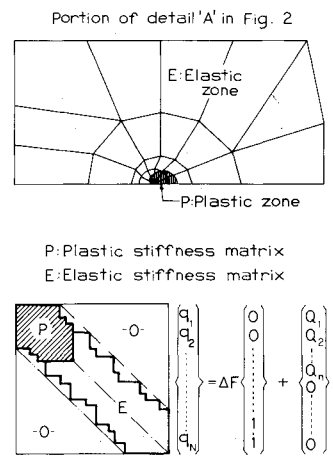

Fig. 3 Representative yield zone at σ_{max} and schematic representation of incremental equations in the presence of yielding.

Techniques to Minimize Computational (CPU) Time

First we note that, the near-tip elements used presently are of the order of 10^{-1} times the semi-crack-length, and the total number of algebraic equations for the above problem is only 311. For the presently considered levels of applied far-field stresses, only "small-scale" yielding conditions prevail near the crack tip, as shown in Fig. 3 for a typical case of presently considered mode I loading. Thus the constitutive properties of only the plastic region (designated in Fig. 3 as region P, and which is much smaller than the elastic region, region E) need to be changed in each load step and/or each iteration. Moreover, in the present class of problems, the finite deformation effects can be seen to be predominant only in the region of the crack tip. For this reason, even though the general formulation presented in Eq. (1) is for finite deformations, the changes in the stiffness of region E due to finite deformation effects are ignored. Thus, only the stiffness matrix of region P needs to be changed in each load step and/or iteration.

However, the total number of times, say N, that the combined stiffness matrix (for regions P and E) must be inverted in the course of analyzing a typical problem, say the case of fatigue crack growth under constant amplitude loading, is $N = [(\text{no. of iterations/cycle}) \times (\text{no. of load increments/cycle}) \times (\text{no. of load cycles})]$. For a typical problem, say eight cycles of constant amplitude loading, a typical value for N can be $N = 4 \times 28 \times 8 = 896$. This represents a rather enormous amount of computing; hence a more economical way of solving the stiffness equations is mandatory. Such an economy is affected in the present procedure by: 1) appropriately numbering the nodes so that the stiffness of the region P can be arranged as a small subset of the global stiffness; 2) using a static condensation procedure to first eliminate the equations corresponding to the nodes in region E in the very first load increment; and 3) operating only on the equations for the nodes in region P after the first load-step. Thus, in the example cited above, in all but one of the 896 solutions the number of equations being solved is rather very small.

Monitoring of Crack Closure and Opening in Finite Element Model

Let us assume that, at a given instant of time (at a given point in the loading history), the locations of the crack tip, of the four nodes on the radial line (which coincides with the crack surface) of the singular sector element, and of all other nodes on the crack axis, as well as the current (deformed) profile of the crack surface, are known. We denote the current nodes on the crack surface as "updated Lagrangian nodes." Let us now assume that the crack tip is now further extended by an arbitrary amount (Δa) and the structure is then subjected to further loading. We first note that, in the present development, the boundary displacement (in the direction of the applied normal stress) along a radial line of a "singular" sector element is of the form given in Eq. (3). Using that equation, and knowing, a priori, the radial coordinates (i.e., r as measured from the current crack tip), of the respective nodes on the radial line of the sector element in its immediately previous location, one can compute the values of Δv at the above-mentioned "updated Lagrangian nodes." By

‡This assumption may not strictly be valid, and the triaxiality of the stress state near the crack tip may have to be accounted for in a more rigorous analysis. Such computations, accounting for stress-triaxiality, are, in general, beyond the scope of current computational capabilities.

adding (or subtracting, as the case may be) these incremental displacements to the previously known values, an accurate prediction of the current crack surface deformation profile is made.

During the unloading part of any cycle in the present case, at the instant the displacement (in the direction of applied tension) at one or more nodes on the crack surface becomes negative, further unloading is stopped. The computational procedure is then switched to a displacement control type, and the above negative displacements are precisely enforced to be zero; thus finding the precise stress level at which the closure constraint on the respective node must be enforced.

After the crack closure is detected, the respective node (s) is constrained thereafter, until the restraining force (s) at the node (s) just becomes zero and begins to be tensile in nature. The corresponding applied stress level defines the crack-opening stress. The details of this process are discussed and graphically illustrated elsewhere.[12,14] Finally, some comments on the presently observed patterns of crack closure are given, before proceeding to a discussion of specific cases. In general, closure was noticed to occur at the node closest to the current crack tip, as indicated in the sequence of unloading steps in Figs. 4a-c. However, if the current crack-surface profile is irregular, as in the case of high-to-low block loading, crack closure may first occur at the node closest to the crack tip; however, in the subsequent unloading step, closure may occur at a node far removed from the crack tip, as indicated in Fig. 4d. From the results to be discussed later, this pattern of crack closure appears to contribute significantly to growth retardation and delay effects.

Criterion for Crack-Extension Stress Level

In prior literature, this crack-extension stress level was chosen arbitrarily. For instance, in Ref. 5 the crack is extended at the maximum applied stress in each cycle even in a general spectrum loading (for instance, high-to-low, low-to-high, etc.), whereas in Ref. 7 the crack was extended at the applied stress level at which the restraining nodal force as the new crack tip becomes zero. In the present study, e.g., in a constant-amplitude (zero-to-tension) cyclic loading, it was found that the crack opening and closure stresses, σ_{op} and σ_{cl} respectively, were sensitive to the chosen σ_{ex}. In the present work, a criterion, $\sigma_{ex} = \sigma_{op} + p(\sigma_{max} - \sigma_{op})$ where p is a constant of proportionality, is postulated; and p is obtained by calibration such that the calculated σ_{op} correlated with that observed in experimental studies such as in Ref. 2. However, it is noted that this constant of proportionality p may, to some extent, be dependent on the numerical methodology employed in fatigue crack modeling itself. Thus, the above described calibration may be considered as valid only in the context of the particular methodology employed in the present work. Three different test cases, each with a different magnitude of constant amplitude (zero to tension) cyclic loading, were studied with different values being chosen in each case for the above-mentioned constant of proportionality p. The idea was to select a p that yields results, in each case, for $(\sigma_{op}/\sigma_{max})$ that are in best agreement with the experimental results[2] for 2024-T3 aluminum alloy, which is the material simulated in analysis. The results, for instance, for the case $(\sigma_{max}/\sigma_{ys} = .40)$ and $(R = \sigma_{min}/\sigma_{max} = 0)$ are summarized in Table 1.

Similar results were obtained for the cases, $(\sigma_{max}/\sigma_{ys}) = .229$ and $(\sigma_{max}/\sigma_{ys}) = .314$. From these three sets

Table 1 Dependence of leveled off σ_{op} on p

p	Leveled off σ_{op}, MPa	$[\sigma_{op}/\sigma_{max}]$ at steady state
1.0	115	0.82
0.85	94	0.67
0.62	79	0.56
0.40	58	0.41

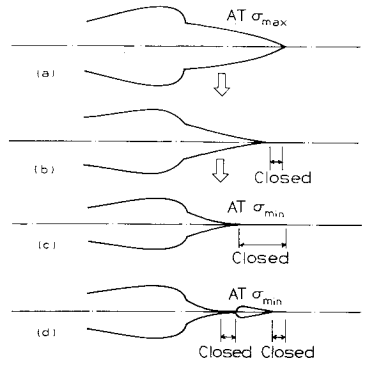

Fig. 4 Representative patterns of crack closure: (a-c) crack tip closes only at nodes closest to crack tip; d crack closure also occurs at nodes away from crack tip.

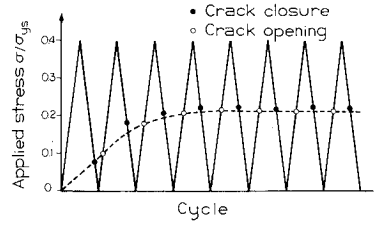

Fig. 5 Crack closure and opening stresses in constant amplitude cyclic loading.

of results, it was observed that $p \sim 0.62$ yields results for $(\sigma_{op}/\sigma_{max})$ that are in the best agreement with experimental observations, which indicate that $[\sigma_{op}/\sigma_{max}]$ at steady state is about 0.56. It is hypothesized that the above constant $p = 0.62$ may be used throughout the rest of the analysis, i.e., for cases of general spectrum loading.

Constant Amplitude Zero-to-Tension Cyclic Loading

The results for σ_{op}, for the case of $(\sigma_{max}/\sigma_{ys}) = 0.4$ and $R = (\sigma_{min}/\sigma_{max}) = 0$, are shown in Fig. 5, for eight cycles of loading. It is observed that σ_{op} reaches a "steady-state" value of 0.56 σ_{max} after the fourth or fifth cycle. It is also noted that this value for σ_{op}/σ_{max} $(=0.56)$ is in reasonable accord with experimental results[2] for the same material, a 2024 T3 aluminum alloy. Knowing σ_{op} in each cycle, we define the effective stress-intensity factor as:

$$\Delta K_{eff} = C_I \sqrt{\pi(a_0 + N\Delta a)}\,(\sigma_{max} - \sigma_{op})$$

where C_I is the finite-size correction factor for the present crack geometry (which was found to be $C_I = 1.017$ from a finite element linear analysis of the crack with $a = a_0$; and thereafter assumed to be constant); N is the number of cycles and Δa is the crack growth per cycle. It is thus seen that ΔK_{eff} levels off after a few cycles to a steady-state value.

Figure 6 shows the crack surface deformation profiles at various stages of unloading during the eighth cycle of the present constant-amplitude $(R = 0)$ cyclic loading. The large blunting at the initial crack-tip location $(a = a_0)$ is observed to remain permanently. The surface of the extended crack is observed to be fairly smooth. During the eighth cycle, it is observed that precise crack-closure occurs only over the area Δa (i.e., only at the previous location of the crack-tip node) even upon full unloading; however, it is also noted that, at this stage, the opening of the crack faces between the points a_0 and the precisely closed node is very small (see Fig. 6).

Low-to-High Block Loading

A two-level block loading, from low to high, with σ_{max} in the higher level being 1.273 times the σ_{max} in the lower level, is considered. The maximum stress in the lower level is taken such that $(\sigma_{max})_{low} \div (\sigma_{ys}) = 0.314$. As mentioned earlier, the

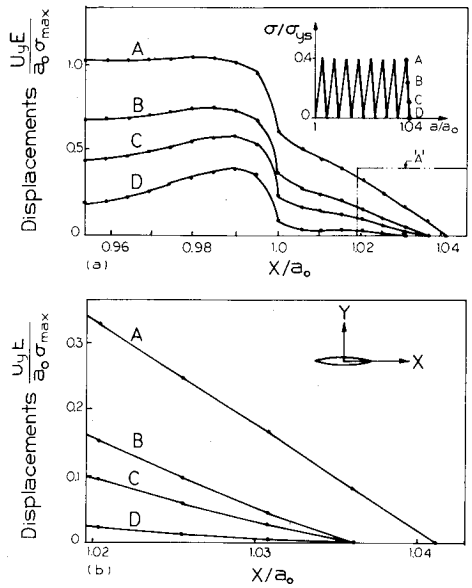

Fig. 6 a) Crack-line profile during unloading in constant-amplitude loading; b) magnification of insert A.

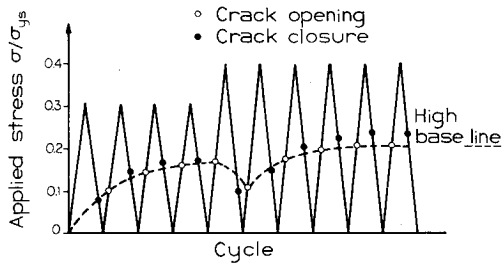

Fig. 7 Crack closure and opening stresses in low-to-high block loading.

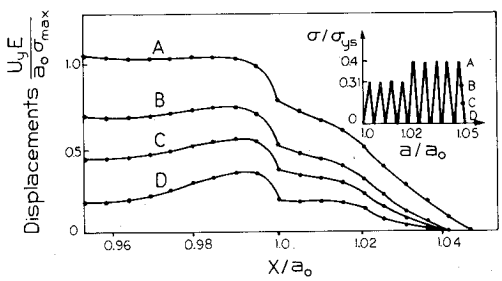

Fig. 8 Crack line profile during unloading in low-to-high block loading.

data at the end of four cycles of low-level block loading (see Fig. 7) are recovered from a constant-amplitude test case, with the corresponding stress level. The following results were obtained:

1) The variation of crack-opening stress, σ_{op}, as the cyclic loading progresses, is shown in Fig. 7. It can be seen that immediately after the step up in the level of applied stress, σ_{op} decreases by about 33% of its steady-state value corresponding to the lower level of block loading. Subsequent to this, σ_{op} increases monotonically to a steady-state value corresponding to the higher level of block loading, within about five cycles. Prior to this stabilization, ΔK_{eff} (defined as before) in the higher level of block loading remains considerably higher than the steady-state value corresponding to this stress level, thus indicating growth acceleration following the load step-up.

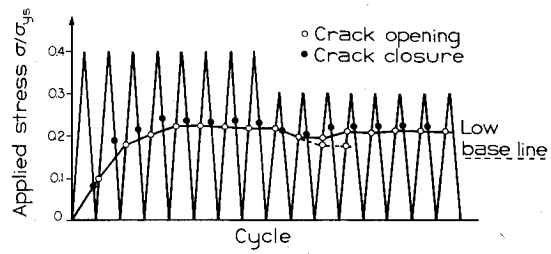

Fig. 9 Crack closure and opening stresses in high-to-low block loading.

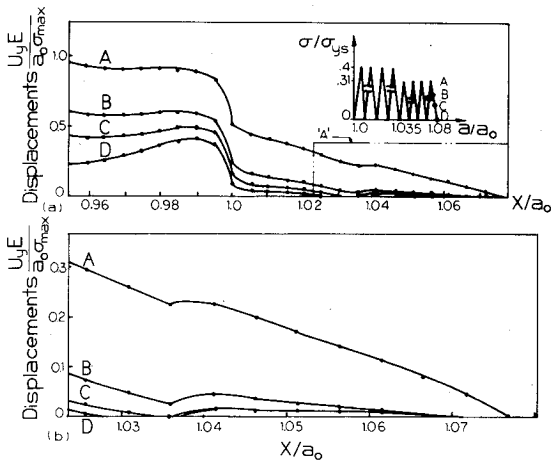

Fig. 10 a) Crack line profile during unloading in high-to-low block loading; b) magnification of inset A.

2) The representative crack surface profiles, e.g., at various stages of unloading at the end of the eighth cycle (high stress) of the current low-to-high level block loading, are shown in Fig. 8. From this figure, it can be seen that the step-up in the level of loading causes a blunting of the crack tip (i.e., at the location $x/a = 1.02$ in Fig. 8, when the step-up in loading occurs in the present finite element simulation). Even during the unloading, as seen from Fig. 8, the crack-closure occurs only over the area Δa (i.e., only at the previous location of the crack-tip node).

High-to-Low Block Loading

After eight consecutive cycles of a high-level block loading (at which point the data are recovered from the corresponding constant amplitude test case), σ_{max} was reduced by 21.4% and eight more cycles of this reduced level block loading were considered. The magnitude of the applied stress in the high-level block was such that $(\sigma_{max})_{high} \div \sigma_{ys} = 0.40$. The following results were obtained.

1) The variation of the crack-opening stress σ_{op} as the loading progresses is shown in Fig. 9. It is seen that, immediately after the step-down in the load level, no abrupt decrease in σ_{op}, as was the case in low-to-high loading, occurs in the present high-to-low block loading case. After the load-level step down, σ_{op} stayed at about 0.70 $(\sigma_{max})_{low}$ within the number of cycles of low-level load presently considered. It may be possible that as a larger number of low-level load cycles is considered and the crack tip grows further and eventually surpasses the plastic zone created during the high level block loading, the σ_{op} may decrease to a baseline value corresponding to the lower level block loading. However, limitations of computer funds precluded the possibility of considering a larger number of load cycles at the low level. It is also seen that after the load-level step-down, ΔK_{eff} remains remarkably lower than its baseline value corresponding to the low-level block loading, thus indicating the presence of a considerable retardation of growth, but no delay.

Table 2 Three cases of single overload

Case	Base σ_{max}, MPa	$\frac{\sigma_{overload}}{\sigma_{max \cdot base}}$	$\frac{\sigma_{op_{max}} - \sigma_{op.base}}{\sigma_{max \cdot base} - \sigma_{op \cdot base}}$
1	110	1.273	0.151
2	110	1.455	0.283
3	80	2.0	0.681

2) Figure 10 shows the crack surface profiles during various stages of unloading in one of the low-level cycles of the present high-to-low block loading. It is seen that at the stage of unloading indicated by point B in Fig. 10, the crack closes only at the previous crack tip (closure area $= a$). Further unloading, represented by point C, causes another node away from the current crack tip to close, as seen in Fig. 10. The area of crack closure thus increases as the unloading progresses.

To understand the effects of the features of crack closure as in the present case, the problem was reanalyzed with the constraint of closure removed on the node (as discussed above) far away from the crack tip, but leaving the closure-constraint on the node closest to the crack tip. The corresponding changes in σ_{op} are indicated by a broken line in Fig. 9. The results indicate the influence of properly imposing the closure constraints on nodes even far away from the crack tip when the considered loading, as the present high-to-low case, causes such a type of crack-closure.

Single Overload

The case of a single overload after four cycles of a constant-amplitude block loading, followed by further cycles of constant amplitude (equal in magnitude to that before overload) was considered. The three cases considered are shown in Table 2.

In this table, $\sigma_{max\ base}$ is the maximum applied stress prior to or after overload; $\sigma_{overload}$ is the overload stress; $\sigma_{op\ max}$ is the maximum calculated value for crack-opening stress after overload; and $\sigma_{op\ base}$ is the baseline opening stress for an otherwise constant-amplitude cyclic load at level $\sigma_{max\ base}$. All of these stresses are illustrated in Fig. 11. The results obtained are as follows.

1) The variations of σ_{op} during the load cycling, for the three different ratios of stress overload, are indicated in Figs. 11a-c, respectively. In all three overload cases an abrupt decrease in σ_{op} (whose relative decrease becomes more predominant as the overload stress ratio increases) is noticed immediately after the single overload application. After this, in all three cases, σ_{op} increases again to reach a peach value $\sigma_{op\ max}$ before leveling off to a steady-state value. The relative values of $\sigma_{op\ max}$ increase as the overload stress ratio increases. Also, as the overload stress-ratio increases, the latter is the occurrence of this $\sigma_{op\ max}$. For instance, for the overload stress-ratio of 1.273, $\sigma_{op\ max}$ occurs in the fourth cycle after overload (Fig. 11a); for an overload ratio of 1.455 this occurs in the eighth cycle after overload (Fig. 11b); while for the case of overload ratio 2.0, σ_{op} is still increasing (Fig. 11c). This implies that the higher the overload ratio is, the more remarkable both the retardation and delay effects are. This conclusion is in accord with the observation of Schijve,[1] based on the experimental results of Arkema.[15]

2) It is seen that ΔK_{eff} experiences a sudden jump immediately after the overload, and then decreases below its baseline level corresponding to a constant-amplitude cycling at the $\sigma_{max\ base}$ level; thus indicating the presence of retardation and delay effects (these terms are used here in the same sense as defined by Bernard et al.[16]) in this single overload case. It is also noted that the quantitative effects of retardation and delay depend on the overload ratio.

3) The curve depicting the variation of the ratio $(\sigma_{op\ max} - \sigma_{op\ base})/(\sigma_{max\ base} - \sigma_{op\ base})$ with the overload stress ratio,

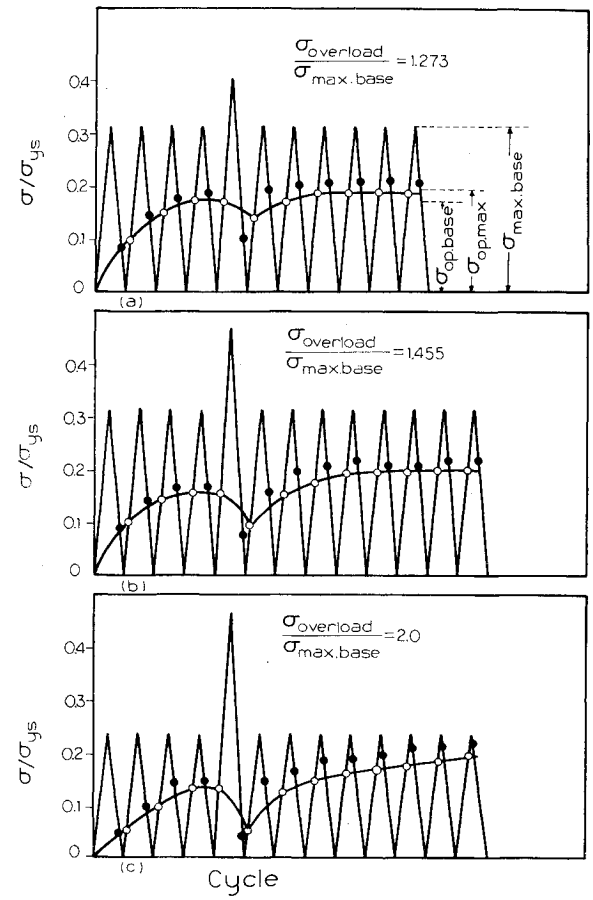

Fig. 11 Crack closure and opening stresses for three different cases of a single overload.

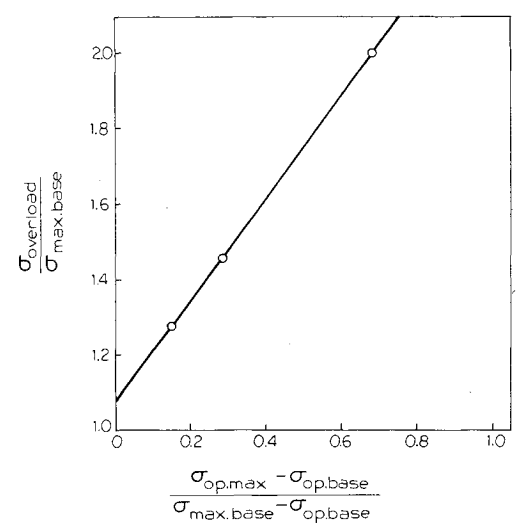

Fig. 12 Effect of overload stress ratio on $(\sigma_{op\ max} - \sigma_{op\ base})/(\sigma_{max\ base} - \sigma_{op\ base})$.

which is drawn using the above discussed three data points, is shown in Fig. 12. By extrapolation, the threshold value of the overload ratio, at which retardation effects come into play, is about 1.10. In contrast, Bernard et al.[16] report a threshold overload ratio of 1.3 ~ 1.4 based on a series of experiments on Ducol W30B, whose yield strength is 366 MPa (comparable to the presently considered $\sigma_{ys} = 350$ MPa). It is noted, however, that the present analysis is based on a plane-stress assumption, while Bernard et al.[16] note the dependence of the experimentally determined threshold value on the specimen thickness.

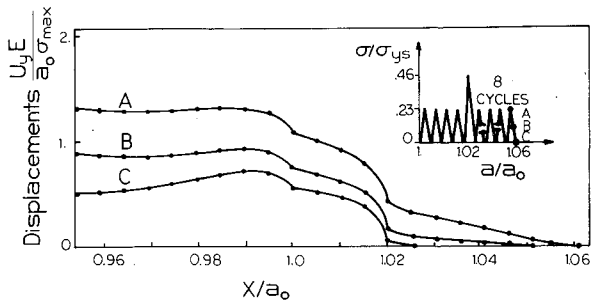

Fig. 13 Crack line profile during unloading after a single overload.

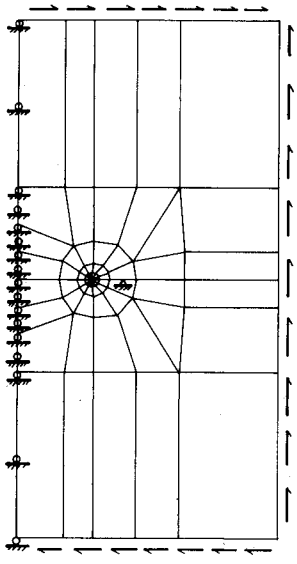

Fig. 14 Geometry and finite element model of a center-cracked panel under pure shear cyclic loading.

4) The crack-line deformation profiles at various stages of unloading at the end of the considered number of cycles are shown in Fig. 13 for the case of overload ratio of 2, while similar results were also noted for the other tow overload ratio cases. It is seen that the application of the single overload to the specimen (at the instant when $a/a_0 = 1.02$ in Fig. 13) causes a large (plastic) blunting which is retained in the crack-surface profile even as the crack advances in further cyclic loading. When the specimen is fully unloaded, at the end of the cycle illustrated in Fig. 13, almost the whole surface area ahead of the previously mentioned location of blunting is noticed to close, while the crack surface area behind this blunting location is seen never to close.

Analysis of a Center-Cracked Specimen Under Pure Mode II Cyclic Loading

A center cracked square plate under a constant amplitude cyclic loading of pure shear, which is uniformly distributed at the edges of the plate, is analyzed. Plane stress conditions are assumed. The material is 2024-T3 aluminum alloy. The dimensions of the plate are: $L = W = 140$ mm; $a_0 = 40$ mm. The maximum amplitude of the uniformly distributed shear is taken to be $\tau_{max} = 80$ MPa ($\tau_{max}/\sigma_{ys} = 0.23$). In the present problem, the geometry of the plate with the crack is symmetrical about both the x and y axes (see Fig. 14), and the external loading is antisymmetric with respect to both x and y axes. As earlier, the present material is modeled as an elastic-perfect-plastic material. We note also that the presently considered material has the same properties in tension as in compression. Only a half of the plate is modeled as shown in Fig. 14. The linear elastic results, based on the first load increment, indicate: $K_I = 0.075$, and $K_{II} = 3.777$, while the corresponding results cited by Bowie and Neal[17] are: $K_I = 0.0$, and $K_{II} = 3.899$. The fact that $K_I \neq 0$ in the present analysis is

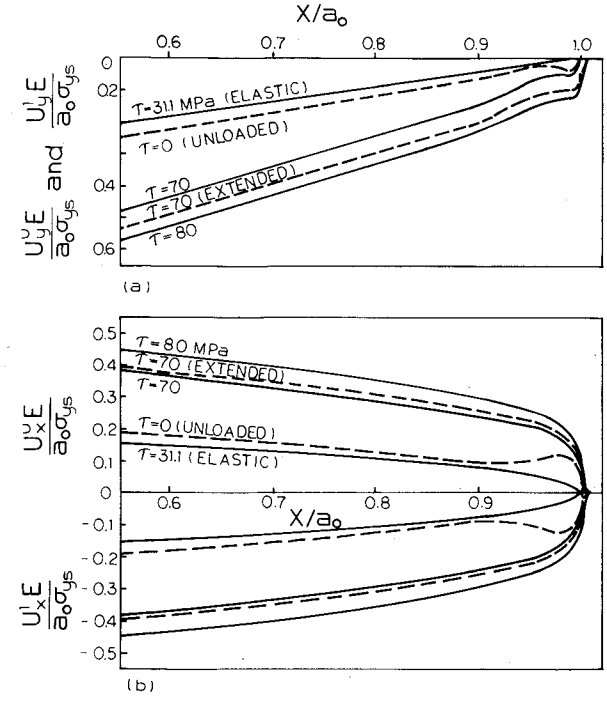

Fig. 15 a) Normal displacement profiles of upper and lower surfaces of the crack; b) tangential displacement profiles of upper and lower surfaces of the crack.

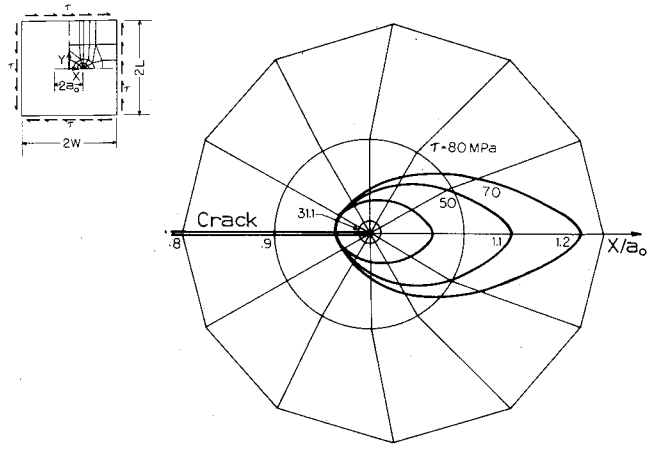

Fig. 16 Plastic zone near crack tip in a center-cracked panel under pure shear cyclic loading.

the result of inherent numerical errors in the present finite element procedure. In fatigue analysis the crack was assumed to extend at $\tau = 70$ MPa, for lack of any other valid criteria.

In Fig. 15a the results for the displacements u_y at the upper and lower crack surfaces, u_y^u and u_y^l respectively, are plotted. These results are presented for the following cases: 1) at $\tau = 31.1$, when linear elastic conditions prevail almost throughout the plate; 2) at $\tau = 70$ MPa, before and after crack extension; 3) at $\tau_{max} = 80$ MPa in the loading cycle; and 4) at the completion of unloading, $\tau = 0$. It is seen that in all of these cases, the numerical results for u_y^u and u_y^l are almost identical in magnitude and sign. Similar results for u_x^u and u_x^l are shown in Fig. 15b, from which it is again seen that u_x^u and u_x^l, for all the above mentioned values of τ, are identical in magnitude but opposite in sign. A more detailed discussion of these results can be found in Ref. 18.

These results show that, for the presently considered cases of homogeneous materials with identical properties in tension as in compression, in all cases of loading, crack growth, and unloading, the upper and lower surfaces of the crack move

together in the direction perpendicular to the initial crack axis, while they slide past one another in the direction of the crack axis. Thus, for these types of materials, the phenomenon of crack closure, as observed experimentally and as analyzed presently in mode I conditions, does not occur in pure mode II cyclic loading. However, the present experience also indicates that crack closure may occur even in mode II cyclic loading if the material has different properties in uniaxial tension and compression. Such materials are not pursued in the present work.

Finally, the computed shapes and sizes of the plastic zones near the crack tip are shown in Fig. 16.

Summary and Conclusions

If the crack-growth rate, da/dn, in mode I fatigue loading can be assumed to be related the effective stress-intensity range K_{eff} the present results indicate that: 1) growth retardation occurs in high to low and single overload cases; and 2) significant delay effects prior to retardation occur in the case of a single overload and these delay and retardation effects become more predominant as the overload ratio increases. From the crack surface deformation profiles shown in Figs. 8 and 13, it is seen that a considerable crack-surface blunting occurs at the instant when the applied load is stepped up. This blunting at the instant of load step-up alters the possible pattern of crack closure during subsequent load cycles, and is seen to be responsible for the "delay" effects such as the delayed retardation in the single-overload case, and the delayed transition of opening stress levels from the baseline values for lower amplitude block loading to the higher baseline value for the higher amplitude block loading in the low-to-high case. The physical mechanism behind these effects is further detailed in Refs. 12 and 14. Finally, the phenomenon of crack closure was not observed in the present numerical modeling of a thin center cracked sheet (of an elastic-plastic material with identical properties in uniaxial tension as in compression), subject a pure shear (mode II) cyclic loading of constant amplitude. Thus, it appears that, in the study of the more general problem of fatigue crack-growth under mixed-mode loading which causes small scale yieldings near the crack tip, crack-closure effects need be considered in the mode I component only. However, the present experience indicates that crack closure may occur even in pure mode II if the material has different properties in uniaxial tension and compression.

Acknowledgments

This work was supported in part by NASA Grant No. NSG-1351 and by AFOSR Contract No. F49620-78-C-0085. This support is gratefully acknowledged.

References

[1] Schijve, J., "Four Lectures on Fatigue Crack Growth," *Engineering Fracture Mechanics,* Vol. II, No. 1, 1979, pp. 165-223.

[2] Elber, W., "Fatigue Crack Closure Under Cyclic Tension," *Engineering Fracture Mechanics*, Vol. II, July 1979, pp. 37-45.

[3] Budiansky, B. and Hutchinson, J.W., "Analysis of Closure in Fatigue Crack Growth," *Journal of Applied Mechanics*, Vol. 45, June 1978, pp. 267-276.

[4] Newman, J.C. Jr. and Armen, H. Jr., "Elastic-Plastic Analysis of a Propagation Crack Under Cyclic Loading," AIAA Paper 74-366, Las Vegas, Nevada, April 17-19, 1974.

[5] Newman, J.C. Jr., "A Finite-Element Analysis of Fatigue Crack Closure," *Mechanics of Crack Growth*, ASTM STP 590, American Society for Testing and Materials, 1976, pp. 281-301.

[6] Ohji, K., Ogura, K., and Okubo, Y., "Cyclic Analysis of a Propagating Crack and its Correlation with Fatigue Crack Growth," *Engineering Fracture Mechanics*, 1975, Vol. 7, pp. 457-464.

[7] Ogura, K. and Ohji, J., "FEM Analysis of Crack Closure and Delay Effect in Fatigue Crack Growth Under Variable Amplitude Loading," *Engineering Fracture Mechanics*, Vol. 9, 1977, pp. 471-480.

[8] Hutchinson, J.W., "Singular Behavior at the End of a Tensile Crack in a Hardening Material," *Journal of Mechanics and Physics of Solids*, Vol. 16, 1968, pp. 13-31.

[9] Rice, J.R. and Rosengren, G.F., "Plane Strain Deformation Near a Crack Tip in a Power Low Hardening Material," *Journal of Mechanics and Physics of Solids*, Vol. 16, 1968, pp. 1-12.

[10] Atluri, S.N. and Nakagaki, M., "J-Integral Estimates for Strain-Hardening Materials in Ductine Fracture Problems," *AIAA Journal*, Vol. 15, July 1977, pp. 923-931.

[11] Atluri, S.N., Nakagaki, M. and Chen, W.H., "Fracture Analysis Under Large Scale Yielding: A Finite Deformation Embedded Singularity, Elastic-Plastic Incremental Finite Element Solution in Flaw Growth and Fracture," ASTM STP 631, American Society for Testing and Materials, 1977, pp. 43-61.

[12] Nakagaki, M. and Atluri, S.N., "Elastic-Plastic Finite Element Analyses of Fatigue Crack Growth in Mode I and Mode II Conditions," NASA-CR-158987, Nov. 1978.

[13] Atluri, S.N., "On Some New General and Complementary Energy Theorems for the Rate Problems in Finite Strain, Classical Elasto-Plasticity," Georgia Institute of Technology, Rept. GIT-ESM-SA-78 10, Aug. 1978. (in review for publication in *Journal of Mechanics and Physics of Solids*).

[14] Nakagaki, M. and Atluri, S.N., "Fatigue Crack Closure and Delay effects Under Mode I Spectrum Loading: An Efficient Elastic-Plastic Procedure," to appear in *Proceedings of the 3rd International Conference on Mechanical Behaviour of Materials*, University of Cambridge, United Kingdom, Sept. 1979.

[15] Arkema, W.J., results quoted in J. Schijve, "Observations on the Prediction of Fatigue Crack Growth Propagation Under Variable-Amplitude Loading," ASTM STP 595, 1976, p. 3.

[16] Bernard, P.J., Lingley, T.C., and Richards, C.E., "Mechanisms of Overload Retardation During Fatigue Crack Propagation," *Fatigue Crack Growth Under Spectrum Loads*, ASTM STP 595, 1976, pp. 78-97.

[17] Bowie, O.L. and Neal, P.M., "A Note on the Central Crack in a Uniformally Stressed Strip," *International Journal of Fracture Mechanics*, Vol. 2, November 1970, pp. 181-182.

[18] Nakagaki, M. and Atluri, S.N., "An Elastic-Plastic Analysis of Fatigue Crack Closure in Modes I and II," AIAA Paper 79-0758, St. Louis, Mo., 1979.